## PAPER

# One step hydrothermal synthesis of CeO$_2$–ZrO$_2$ nanocomposites and investigation of the morphological evolution†

Xiaohui Zhang,[ab] Qiang Wang,*[ab] Jing Zhang,[ab] Jigang Wang,[ab] Ming Guo,[ae] Shaowei Chen,*[c] Chunhong Li,[d] Changwen Hu[e] and Youchang Xie[f]

Uniform cauliflower-like and rough nano-spheres of CeO$_2$–ZrO$_2$ composites were synthesized by a facile hydrothermal process using only urea as a mineralizer without any surfactant or template. The structural morphologies were found to vary with the reaction time, calcination temperature and dosage of urea and the urea was verified to play an important role in the determination of the CeO$_2$–ZrO$_2$ composite nanostructures. The samples were characterized by X-ray diffraction (XRD), X-ray photoelectron spectroscopy (XPS), scanning electron microscopy (SEM), high-resolution transmission electron microscopy (HRTEM) and other techniques. On the basis of the characterizations, it was proven that there existed migrations or movements during the hydrothermal process especially with long hydrothermal time and a possible mechanism was proposed which would go through a series of procedures of nucleation, Ostwald ripening and Kirkendall effect to account for the structural dynamics and morphological evolutions. Subsequently, the hybrid Ce$_{0.9}$Zr$_{0.1}$O$_2$–GO was reduced by a hydrothermal method, which showed good adsorption for RhB.

## Introduction

CeO$_2$ (ceria) and ceria-based composite materials are important heterogeneous catalysts used extensively in energy conversion and pollution control.[1–3] Interestingly, the incorporation of Zr$^{4+}$ into the CeO$_2$ crystal lattice (formation of solid solution) has been found to result in a significant increase in the reducibility of CeO$_2$ (Ce$^{4+}$ to Ce$^{3+}$).[4–13] The incorporation not only improves the thermal stability of CeO$_2$ and prevents sintering of the resulting Ce$_{1-x}$Zr$_x$O$_{2-\delta}$ solid,[7] but also improves oxygen storage/release capacity (OSC).[14] This incorporation of zirconium can also change the adsorption properties of some material, for example, Zr-stabilized CaO perform better than CaO in term of CO$_2$ capture.[15] Graphene-based hybrids, because of their great usefulness, have attracted much attention in many areas, such as electronics and photocatalysis,[16–18] for example, CeO$_2$–reduced graphene oxide hybrids (CeO$_2$–RGO) composites show good photocatalytic activity for degradation of rhodamine B (RhB) under UV-light irradiation.[47]

It is well known that catalytic activity strongly depends on the morphologies of the catalysts. For CeO$_2$ and ZrO$_2$, a variety of morphologies have been prepared *via* well-developed routes, including nanoparticles, octahedra, nanotrigulars, *etc.*[19–27] The typical synthetic methods for CZ composites include coprecipitation, high-temperature calcination, high-energy mechanical milling, surfactant-assisted synthesis, micro-emulsion, sol–gel technique, and chemical filing.[28–32] Among these methods, hydrothermal synthesis has been regarded as one of the most effective and economical routes, because of its low-temperature operation, and ease of shape control. However, it remains an important challenge to develop facile, economical, and effective methods for the preparation of functional composites with controllable architectures and to investigate the correlation between morphologies and properties.

Based on the existing literatures, many factors have been found to play an important role in the determination of catalyst morphology and the eventual catalytic performance, such as calcination temperature and hydrothermal time.[33–39] In order to find out the reasons for the formation of different morphologies, many groups put forward several methods/phenomena,

[a]Laboratory for Micro-sized Functional Materials & College of Elementary Education, Capital Normal University, 100048 Beijing, PR China. E-mail: qwchem@gmail.com; Fax: +86 10 68901751; Tel: +86 10 68902523

[b]Department of Chemistry, Capital Normal University, 100048 Beijing, PR China

[c]Department of Chemistry and Biochemistry, University of California, Santa Cruz, CA 95064, USA. E-mail: shaowei@ucsc.edu; Fax: +1 831 5027264; Tel: +1 831 4595841

[d]National Laboratory for Superconductivity, Institute of Physics and Beijing National Laboratory for Condensed Matter Physics, Chinese Academy of Sciences, 100190 Beijing, PR China

[e]Key Laboratory of Cluster Science of Ministry of Education of China, The Institute for Chemical Physics and Department of Chemistry, Beijing Institute of Technology, 100081 Beijing, PR China

[f]College of Chemistry and Molecular Engineering, Peking University, 100871 Beijing, PR China

such as the Kirkendall effect, Ostwald ripening, and the template method.[40–43]

Despite these early partial successes in the aspect of morphology control and the adjustments of catalytic performance, there remain challenges, in particular, in the synthesis of CZ of controlled morphologies from simple starting materials. Moreover, clear explaining the mechanism related to the morphology in the synthesis process was still a challenge. Therefore, the aim of the present study is to identify and examine the experimental control of the structural morphology of CZ. Experimentally, a hydrothermal procedure was employed to synthesize CZ composites by using urea as the starting material but without any additional surfactant and template. The impacts of several experimental parameters were carefully studied, such as the reaction time and temperature and reactant initial feed ratio, on the crystallinity and morphology of the nanopowders. The integrated description for the contribution to the formation of flower-shaped CZ spheres based on the Ostwald ripening and Kirkendall effect were speculated. $Ce_{0.9}Zr_{0.1}O_2$–GO hybrids have been also prepared by using the hydrothermal method, which performed good adsorption for rhodamine B (RhB).

## Experimental

### Materials

Cerium(III) nitrate hexahydrate ($Ce(NO_3)_3 \cdot 6H_2O$, AR, Tianjin Guangfu Fine Chemical Research Institute), zirconium nitrate hexahydrate ($Zr(NO_3)_4 \cdot 5H_2O$, AR, Sinopharm Chemical Reagent Co., Ltd) and urea (Beijing Tong Guang Fine Chemical Company) were of analytical grade and used without further purification. Distilled water was purified with a Milli-Q system (Millipore, Billerica, MA).

### Preparation of CZ composites nanomaterials

In a typical synthesis, 4.5 mmol of $Ce(NO_3)_3 \cdot 6H_2O$, 0.5 mmol of $Zr(NO_3)_4 \cdot 5H_2O$ and a certain amount of $CO(NH_2)_2$ (urea) were dissolved in 70 mL of deionized water, sufficiently stirred. The homogenous solution was transferred into a 100 mL Teflon-lined autoclave, which was sealed and maintained at an appropriate temperature (373 K for 10 h or 48 h). After the autoclave was cooled to room temperature, the resulting white precipitate was collected, washed several times with distilled water and absolute ethanol and dried overnight at 353 K. The white precipitate was finally calcined in air at 673 K for 5 h.

Samples at different ceria to zirconia molar ratio were also prepared in a similar fashion. The resulting products were denoted as $Ce_{0.9}Zr_{0.1}O_2$, $Ce_{0.75}Zr_{0.25}O_2$ at the molar ratio of Ce/Ce + Zr = 0.9, Ce/Ce + Zr = 0.75, respectively.

### Characterization of CZ composite nanomaterials

The composition, morphologies and structures of the CZ nanopowders prepared above were characterized by X-ray powder diffraction (XRD, Bruker D8, Cu Kα radiation, λ = 1.54 Å), field-emission scanning electron microscopy (FE-SEM, JSM-7001F, 10 kV), Transmission Electron Microscope (TEM,

Hitachi-7650) with the acceleration voltage of 80 kV. The transmission electron microscopy images and the corresponding selected-area electron diffraction (SAED) patterns were taken on a high-resolution transmission electron microscope (HRTEM JEOL 2010F, 200 kV). Nitrogen sorption isotherms of the samples were measured at −196 °C using 3H-2000PS1/2 static volume methods. The specific surface and pore size analysis was produced by Beishide Instrument-ST (Beijing) Co., Ltd. The surface structures of the samples were determined on a constant volume adsorption apparatus by the nitrogen-Brunauer–Emmett–Teller (BET) method at liquid nitrogen temperature. The X-ray photoelectron spectroscopy (XPS) was studied by ThermoFisher Scientific (Thermo Fisher Scientific USA, ESCALAB 250). The X-ray Source was Monochromated Al Kalph 150 W and spot size was 500 μm. And the passing energy was 200 eV for survey and 30 eV for high resolution scans. Lens Mode was LargeAreaXL and Analyser Mode was CAE. All binding energies were calibrated using contaminant carbon (C1s = 284.8 eV) as a reference. Survey sputtered @ 3 kV, 2 μA, 4 mm. The UV curves were obtained on UV2600 and the wavelength range was 400–700 nm.

## Results and discussion

It is well-known that calcination temperature in the synthesis plays an important role in determining catalyst morphology and the eventual performance. Herein, a series of CZ were synthesized by hydrothermal treatment at 373 K for 48 h and then calcined at elevated temperatures (773 K and 1173 K). XRD measurements of the resulting samples (Fig. 1) exhibited a series of well-defined peaks at $2\theta$ = 28.5, 33.0, 47.5, 56.3, 59.1, 69.4, 76.8 and 79.1°, which might be ascribed to diffractions of the (111), (200), (220), (311), (222), (400), (331), and (420) crystalline planes of face-centered cubic (fcc) $CeO_2$, respectively (JCPDS 43-1002). That is, the composites belonged to $Fm3m$
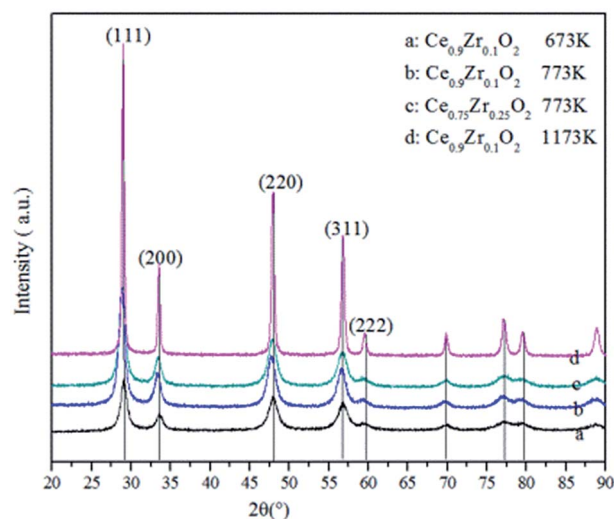


Fig. 1 XRD patterns of CZ (a) $Ce_{0.9}Zr_{0.1}O_2$, (b) $Ce_{0.9}Zr_{0.1}O_2$, (c) $Ce_{0.75}Zr_{0.25}O_2$ and (d) $Ce_{0.9}Zr_{0.1}O_2$, prepared hydrothermally at 373 K for 48 h, then calcined at 673 K, 773 K, 773 K, 1173 K, respectively.
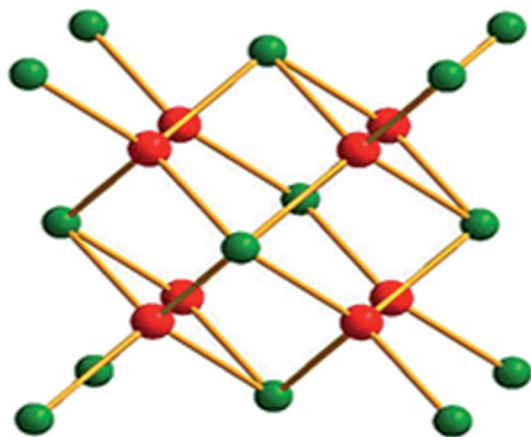
Fig. 2  Model structures of CZ. The red, green colors represent oxygen and CZ atoms, respectively.

[225] with the cell parameters of $a = 5.411$ Å. The optimized structure of the CZ was shown in Fig. 2.

In addition, it can be seen that the XRD patterns became sharper and more intense at higher calcination temperature, and no diffraction peak of $ZrO_2$ was observed, suggesting that $ZrO_2$ was most likely incorporated into the $CeO_2$ lattice to form a solid solution.[37,38] Furthermore, the XPS spectra showed the presence of Zr, so which confirmed our conclusions (Fig. 5).

SEM measurements showed that the resulting nano-composites actually exhibited a rough surface and a cauliflower-like structure, as depicted in Fig. 3a and b which showed the representative SEM images of the CZ prepared by hydrothermal treatment at 373 K for 10 h and 48 h after calcination at 673 K respectively. TEM measurements in Fig. 3c clearly showed the solid structure of the rough CZ with the average diameter of about 140 nm. Fig. 3d was the TEM image of the products after hydrothermal reaction time of 48 h, where a similar structure
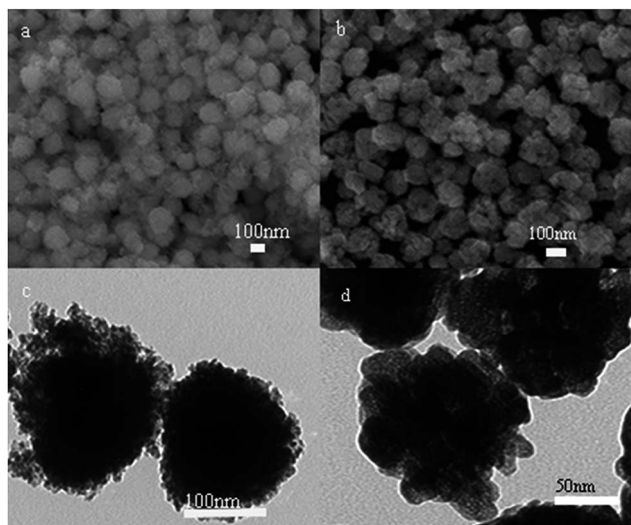


Fig. 3  SEM images of CZ prepared at 373 K for (a and c) 10 h and (b and d) 48 h and then calcined at 673 K.

can be seen but with a less rough surface. The average diameter was somewhat smaller at about 100 nm. This suggested that prolonging calcination time shrank the size of the CZ along with a diminishment of the surface roughness probably because of thermal annealing effects.

In order to observe the changes of the spheres' specific surface area and pore size, the samples were calculated by the $N_2$-BET method. The samples of $Ce_{0.9}Zr_{0.1}O_2$ hydrothermal treated at 373 K for 10 h, 24 h, 48 h then calcined at 673 K, were denoted as A, B, C, respectively. The BET surface area of A, B, C were measured to be 93.7, 79.9 and 66.4 $m^2$ $g^{-1}$, respectively. The average pore width and total volume in pores were collected in Table 1. With the extension of hydrothermal time, the BET surface areas decreased. Interestingly, the average pore size increased first and then decreased. Fig. 4 was nitrogen adsorption–desorption isotherms for the samples. It should be noted that, the isotherms of sample A shown in Fig. 4, showed hysteresis, which were associated to this type of material due to the condensation on capillarities and geometrical morphologies. Sample A displayed hysteresis of type H3 associated to a number of macropores. Besides, the macropores associated to slit aperture may be caused by accumulation of particles. Compared with sample A, there was less number of macropores in sample B, C significantly. The pore size distribution also proved these conclusions (Fig. S1†). Sample B had more micropores than sample A, which may illustrated that there may exit some form of migrations or movement that forced the change in the distribution of the pores. Sample C had more uniform pore size, which may displayed that the migrations or movements may contributed to the formation of regular size products.

In order to detect changes of element content in CZ, the samples were also analyzed by XPS. XPS spectra displayed the signals of the presence of Ce, Zr and O (Fig. 5). The results showed that, all samples' surface were different and the molar ratio of Ce/Zr on the surface of samples A, B, C was showed in Table 2. The molar ratio on sample A surface was 4.44, but that value of sample C surpassed 13. So it could be concluded that the longer of the hydrothermal time was, the higher molar ratio of Ce/Zr would be. And we noted that, after the hydrothermal time of 8 h, the output of product was almost constant and even decreased after calcined at 673 K. These phenomena meant that the content of Zr on the surface of the CZ spheres decreased with the extension of hydrothermal time. Based on the above analysis, there may exit some potential forces that caused to change the distribution of Zr. To prove our conjecture, we

Table 1  Surface area and pore distribution for: $Ce_{0.9}Zr_{0.1}O_2$ hydrothermal treated at 373 K for A: 10 h, B: 24 h, C: 48 h then calcined at 673 K

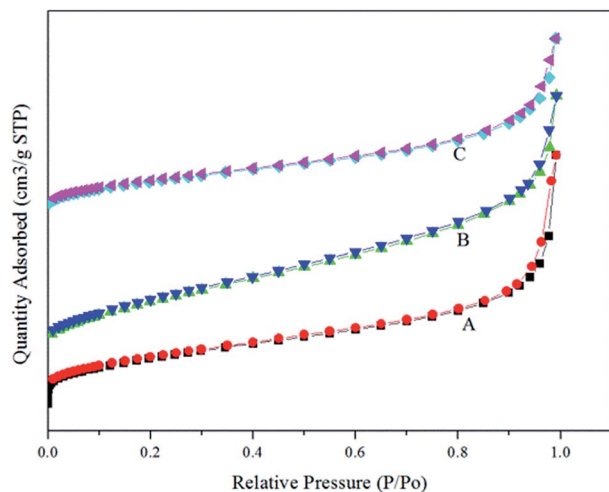|  | A (10 h) | B (24 h) | C (48 h) |
| --- | --- | --- | --- |
| BET surface area ($m^2$ $g^{-1}$) | 93.6745 | 79.9018 | 66.4299 |
| Average pore width (nm) | 8.88067 | 10.51069 | 8.91178 |
| Total volume in pores ($cm^3$ $g^{-1}$) | 0.14014 | 0.14329 | 0.05593 |

Fig. 4 Nitrogen adsorption–desorption isotherms for: $Ce_{0.9}Zr_{0.1}O_2$ hydrothermal treated at 373 K for (A) 10 h, (B) 24 h, (C) 48 h then calcined at 673 K.

**Table 2** The molar ratio of Ce/Zr of: $Ce_{0.9}Zr_{0.1}O_2$ hydrothermal treated at 373 K for A: 10 h, B: 24 h, C: 48 h then calcined at 673 K

| Sample (hydrothermal treated at 373 K for different time) | The molar ratio Ce/Zr |
|---|---|
| A (10 h) | 4.44 |
| B (24 h) | 10.21 |
| C (48 h) | 13.28 |

**Table 3** The molar ratio of Ce/Zr of $Ce_{0.9}Zr_{0.1}O_2$ hydrothermal treated at 373 K for 48 h after sputtered for 30 s, 60 s and 180 s

| Sputtered time of XPS | The molar ratio Ce/Zr |
|---|---|
| 30 s | 123.67 |
| 60 s | 17.64 |
| 180 s | 151.32 |

conducted in-depth analysis of sample C. The sputtering time of the XPS were set to 30 s, 60 s and 180 s, respectively and the results were summarized in Table 3.

From Table 3, we could find that the molar ratio of Ce/Zr varied with different sputtering time significantly. This phenomenon demonstrated that the distribution of inner $Zr^{4+}$ of the CZ spheres varied with the different sputtering time or sputtering depth. Thus, our conjecture was verified that the inward migration of $Zr^{4+}$ to the inner of sphere may come into being. Furthermore, the outward migration of $Ce^{3+}$ happened at the same time. Based on the observation of pure $CeO_2$ (Fig. S2†), it could also be seen the existence of the hollow spheres, which may proved another evidence of the migrations or movements during the hydrothermal process especially with long time under hydrothermal conditions.
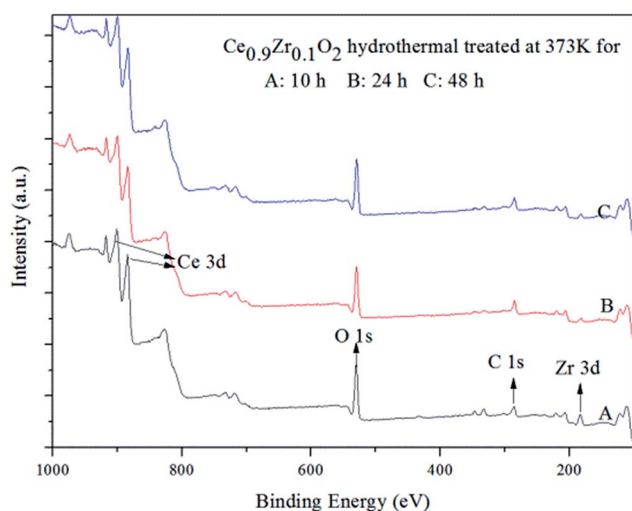


Fig. 5 XPS data: $Ce_{0.9}Zr_{0.1}O_2$ hydrothermal treated at 373 K for (A) 10 h, (B) 24 h, (C) 48 h then calcined at 673 K.

### Effects of reaction time on the morphology of CZ

The structural dynamics of CZ during hydrothermal synthesis was also studied by SEM and TEM measurements (Fig. 6), which exhibited a clear variation with reaction time. Experimentally, after hydrothermal treatment at 373 K for 4 h, a white gel was formed in the solution in the Teflon vessel where the CZ actually contained a number of small nanoparticles, as shown in Fig. 6a. At the reaction time of 6 h, some small nanoparticles grew into long nanowires, where the length can reach over 100 nm (Fig. 6b). When the reaction time increased to 8 h, long nanowires disappeared and concurrently sphere-like particles started to appear (Fig. 6c). The samples obtained after 10 h of reaction were shown in Fig. 6d, where one can see that the rough surface actually entailed tiny particles (about 5 nm). Furthermore, electron diffraction studies indicated that the sphere-like particles were polycrystalline in nature. After 15 h of the reaction, the particles began to shrink (Fig. 6e). At 24 h, one can see the formation of cauliflower-like particles (Fig. 6g), again, with the surface decorated with a stack of particles (Fig. 6f). In comparison, for products obtained at 48 h, the average diameter was actually larger. Fig. 6h showed when the reaction was carried out for 72 h, the shape and size of the CZ became irregular, and the flower-like morphology became less well-defined. Fig. 6i showed the formation of a large number of plenty of smaller particles (diameter less than 100 nm) after 145 h of reaction time. This may be due to thermal instability and hence disintegration of the flower-like structures.

### Effects of the dosages of urea on the morphology of CZ

The effect of the urea dosage was also investigated. The reaction time and temperature were kept constant at 373 K and 10 h or 48 h, and the calcination temperature was kept at 673 K. The molar ratio of urea to precursor was changed from 1 : 1 to 30 : 1. A drastic variation of the surface morphology can be observed. For instance, at the urea to precursor ratio of 1 : 1, no regular morphology was observed after the reaction was carried out for
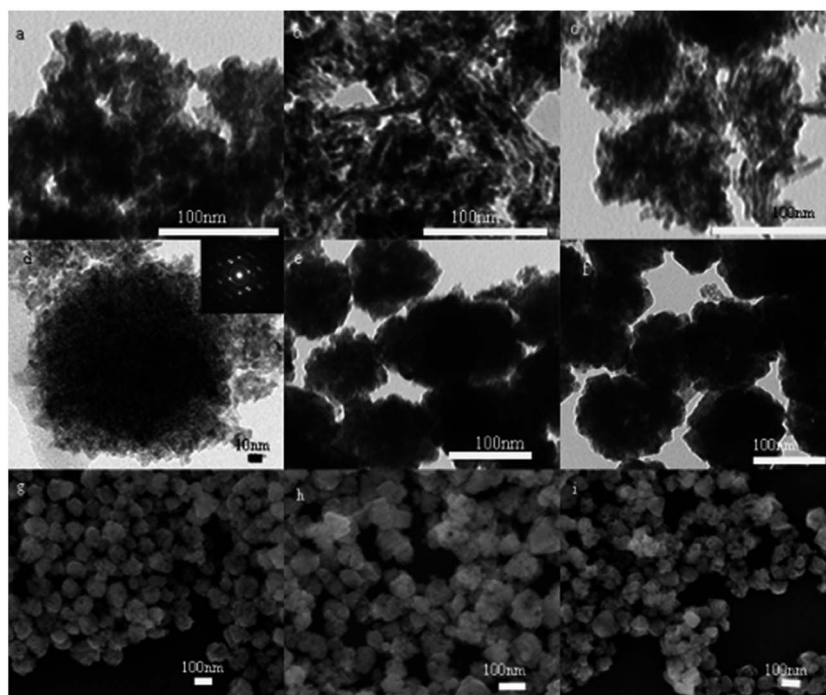
**Fig. 6** TEM images of $Ce_{0.9}Zr_{0.1}O_2$ hydrothermal treated at 373 K for (a) 4 h, (b) 6 h, (c) 8 h, (d) 10 h, (e) 15 h, (f) 24 h; (g–i) SEM images of $Ce_{0.9}Zr_{0.1}O_2$ hydrothermal treated at 373 K for 24 h, 72 h, 145 h and calcined at 673 K.

10 h (Fig. 7a). The main products obtained were rods and particles after the reaction for 48 h (Fig. 7b), where the diameter of the particles was over 500 nm and the length of the rods was over 500 nm along with a cross-section diameter over 100 nm. If the ratio of urea to precursor was changed 10 : 1, 20 : 1 or 30 : 1, the fraction of particles in the final products actually increased accordingly. Prolonging the reaction time to 48 h, the final morphology of the products was different. For instance, at the
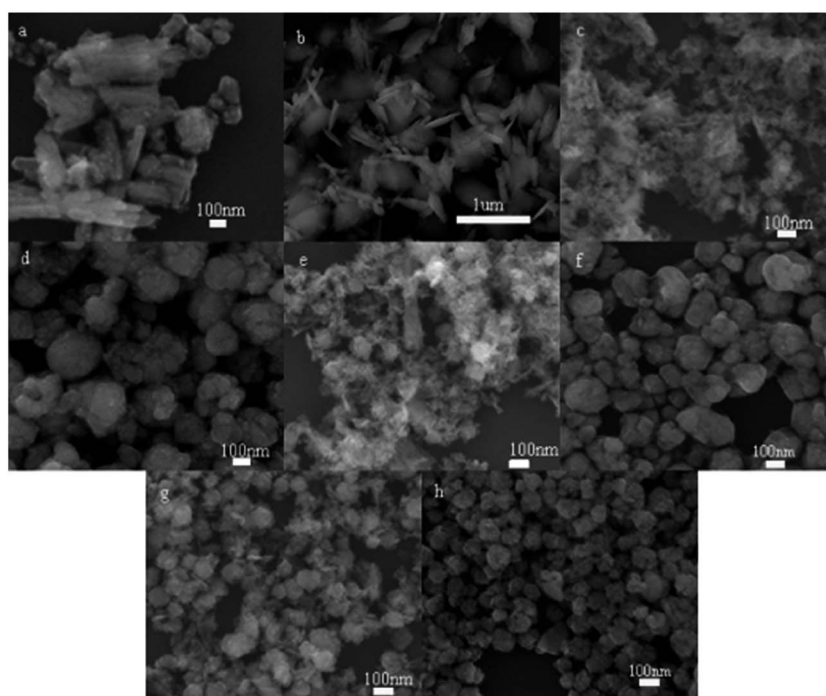


**Fig. 7** SEM images of the $Ce_{0.9}Zr_{0.1}O_2$ hydrothermal treated at 373 K with the molar ratio of urea to precursor was (a) 1 : 1, (c) 10 : 1, (e) 20 : 1, (g) 30 : 1 for 10 h; (b) 1 : 1, (d) 10 : 1, (f) 20 : 1, (h) 30 : 1 for 48 h and calcined at 673 K.

ratio of 10 : 1, all products had rather irregular morphology and size, where the major products were big spheres with a small fraction of tightly packed particles. The average diameter was over 200 nm after 48 h. When the urea to precursor ratio was increased to 20 : 1, the size of the products became more uniform, and the fraction of packed particles became higher. A careful comparison of the regularity and morphology of the products obtained under the ratio 30 : 1 with those under 40 : 1, it was easy to conclude that the two kinds of products were similar in morphology with a small difference in size, implying a similar reaction mechanism in both cases (Fig. S3†). Taken together, the results presented above suggest that the optimal ratio was 40 : 1.

### Effects of temperature on the morphology of CZ

It is well known that hydroxylation of metal ions can be greatly accelerated by raising the solution temperature. Therefore, if the hydrothermal temperature was increased, the kinetics of the formation of the cauliflower-like CZ nanocomposites might be accelerated. This might lead to a drastic change of the CZ morphology, as depicted in Fig. 8. Specifically, very large particles were formed after hydrothermal treatment at 453 K for 10 h. The evolution from particles to wire-like structures was observed at elevated temperatures. At the hydrothermal temperature of 393 K, a mixed product was obtained including rough, sphere-like particles and wire-like structures just after 4 h (Fig. S4a†). Additionally, the fraction of large particles increased with increasing hydrothermal temperature (Fig. S4†).

In addition, the impact of calcination temperature on the morphology of CZ was also examined. The series of experiments were carried out when the urea to precursor ratio was 40 : 1 and the hydrothermal temperature was 373 K. At the calcination temperature of 773 K, the morphology of the final products was still fairly good flower after hydrothermal treated at 373 K for 48 h (Fig. 8f). However, when the calcination temperature was raised to 1173 K, the morphology of products was rather messy with the hydrothermal time of 10 h. One can see the formation of some flower-like particles. This suggested that high temperatures might facilitate the generation of flower-like products. Interestingly, large particles and spheres coexisted at the calcination temperature of 1173 K with the hydrothermal time of 48 h. Similar behaviors were observed at extended hydrothermal times (Fig. S5†).

Furthermore, we also prepared $Ce_{0.75}Zr_{0.25}O_2$ by hydrothermal treatment at 373 K for 48 h followed by calcination at 773 K. It turned out that the morphology did not change apparently after calcination at 773 K (Fig. S6†).

### Possible mechanism for the formation of CZ

From the results presented above, one can see that the dosage of urea, hydrothermal temperature and reaction time were crucial factors that influenced the formation of the CZ with different morphologies. The growth conditions directly determined the final crystal shape. In this experiment, the fact that the change of the crystallite size depended on the urea concentration was mainly explained by the effect of the concentration of hydroxide ion, generated by the decomposition of urea, on the supply of the solute by diffusion and the amount of nucleation.[44] When the concentration of urea was low, the number of urea around $Ce^{3+}$ and $Zr^{4+}$ was very limited in the solution. In the course of the reaction, as a small amount of urea could not provide sufficient hydroxyl groups, nonuniformly sized particles would form, and the shape varied. When the concentration of urea was high, $Ce^{3+}$ and $Zr^{4+}$ were surrounded by a large amount of urea, which facilitated the generation of fine particles. Fine composites particles went through nucleation and grew to linear products, then might aggregate to form large spheres to minimize surface energy. Thus, solid cores were formed at the initial stage of the hydrothermal process. The composite nanospheres at the central core, compared to those at the outer surface, had higher curvature and were easy to be evacuated.[45,46] Therefore, at extended reaction times, the composites nanoparticles aggregated at the central core relocated themselves to the surface to decrease the surface energy during the Ostwald
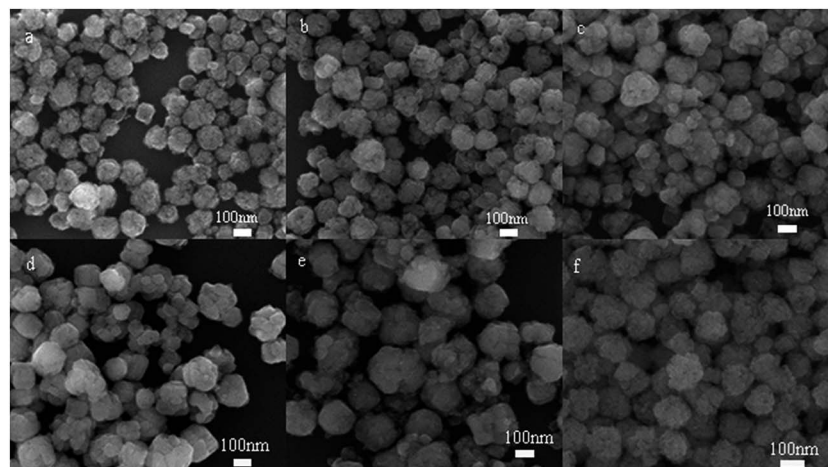


Fig. 8   The molar ratio of urea to precursor was 40 : 1 after hydrothermal treated at (a) 393 K, (b) 413 K, (c) 433 K, (d) 453 K, (e) 473 K for 10 h and calcined at 673 K; (f) hydrothermal treated at 373 K for 48 h and calcined at 773 K.

ripening process, which generated the flower-like structure. On the basis of the above observations, a simple plausible mechanism was proposed for the formation of flower-like products, as depicted in Fig. 9.

Besides, what we should note that, the XPS spectra showed the decreasing Zr amount of the composite with the extension of hydrothermal time, which implied the existence of other factor of migrations or movements apart from Ostwald ripening process.

On this issue, we prepared $Ce_{0.75}Zr_{0.25}O_2$ hydrothermal treated at 373 K for 48 h. Its overall morphology was similar to the sample $Ce_{0.9}Zr_{0.1}O_2$ under the same hydrothermal condition (Fig. S6a†). However, it was difficult to observe the presence of hollow spheres from TEM images (Fig. S6b†). Therefore, we hypothesized that the Kirkendall effect occurred during the hydrothermal process at the same time. The possible mechanism was shown in Fig. 10. Green spheres represented $Zr^{4+}$, red spheres represented $Ce^{3+}$, arrows represented the movement direction of ions. At the beginning, there was a large proportion of $Zr^{4+}$ on the surface of spheres. BET data showed the spheres had a good porosity, which may facilitated the migrations or movements of $Zr^{4+}$ towards the inner of spheres. This migrations or movements in turn made the distribution of pores become uneven gradually. $Zr^{4+}$ migrated into the inner of spheres, while $Ce^{3+}$ had the relatively trend toward the spheres' surface. With the extension of hydrothermal time, there were more components of $Zr^{4+}$ in the sphere as a result of the migration or movement.

Accordance with the above, this migrations or movements included two forms: one was the Ostwald ripening, and the other was Kirkendall effect. During the Ostwald ripening process, the spheres would have good crystal particles and the process may cause the volume shrinkage and the formation of hollow spheres. At the same time, it would cause the aperture become more regular. Furthermore, the Kirkendall effect process would push the diffusion of $Zr^{4+}$ into the inner of spheres. These two migrations or movements exited simultaneously, and jointly promoted the motion of the particles on
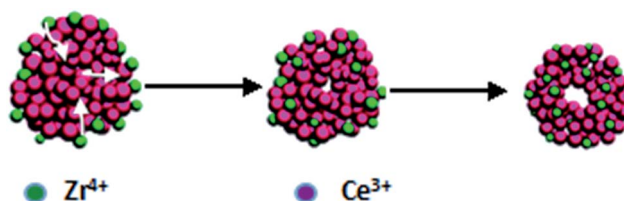
**Fig. 10** Schematic illustration for the change of $Ce^{3+}$ and $Zr^{4+}$ content on flower-like spheres.

spheres. All in all, the combination of these two migrations or movements caused a significant change in spheres' porosity, crystallinity, and morphology. As may be gathered from these analysis, the cross-coupling effects of Kirkendall effect and Ostwald ripening contributed to the formation of flower-shaped spheres.

### The adsorption for rhodamine B

In a typical experiment, graphite oxide (GO) was synthesized by a Hummers method. The $CeO_2$–GO and $Ce_{0.9}Zr_{0.1}O_2$–GO hybrids were obtained *via* a one-step hydrothermal method using supercritical water as green reductant (ESI†).[47] RhB dyes was performed at room temperature and observed based on the absorption spectroscopic technique.

Typically, 15 mg RhB dyes was added into water to get 1000 mL aqueous solution. 30 mg as-prepared samples were dispersed in a 30 mL the as-prepared solution. After ultrasonic dispersion for 20 s, we can find the solution of $Ce_{0.9}Zr_{0.1}O_2$–GO hybrids became purple, the solution of sample $CeO_2$ and $Ce_{0.9}Zr_{0.1}O_2$ were still rather red, however. The results showed that $Ce_{0.9}Zr_{0.1}O_2$–GO had obvious adsorption for RhB, as Fig. 11. The pure GO could also adsorb the RhB, but the adsorption was weak compared with $Ce_{0.9}Zr_{0.1}O_2$–GO. As can be seen from the Fig. 11, the adsorption of $Ce_{0.9}Zr_{0.1}O_2$–GO was higher than the total adsorption of $Ce_{0.9}Zr_{0.1}O_2$ and GO. The incorporation of $Zr^{4+}$ into the $CeO_2$ resulted in the difference at
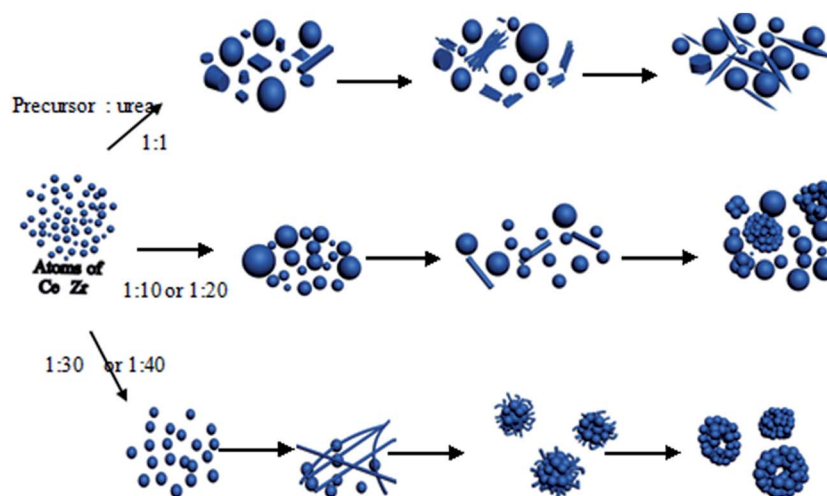
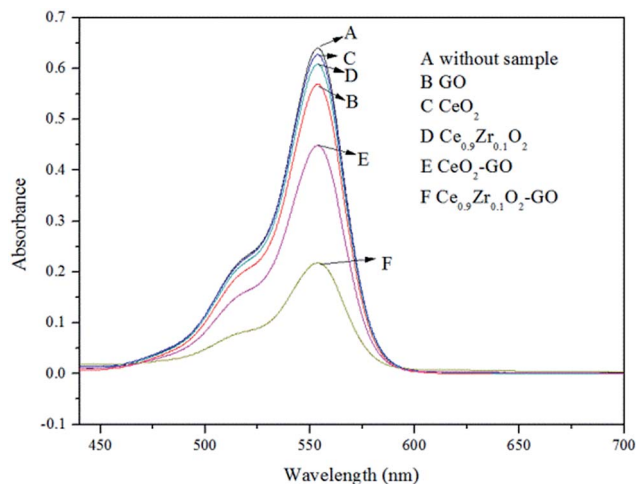**Fig. 9** Schematic illustration for the evolution of flower-like spheres.

Fig. 11 The adsorption activity for RhB (A) without sample, (B) GO, (C) $CeO_2$, (D) $Ce_{0.9}Zr_{0.1}O_2$, (E) $CeO_2$–GO and (F) $Ce_{0.9}Zr_{0.1}O_2$–GO.

the sites of Lewis acid and Brönsted acid.[48] K. Huang *et al.* found that, owing to the introduction of the reduced GO to $CeO_2$, both the adsorption ability for RhB and the separation ratio of photogenerated electron–hole pairs had been greatly enhanced.[47] The possible formation mechanism could be attributed to the initial binding of the $CeO_2$ with GO through carboxyl and oxygen linkages and the subsequent reduction of GO by supercritical water during hydrothermal process *in situ*, which was considered improving the adsorption for RhB.

## Conclusions

In summary, this paper demonstrated a facile method for the synthesis of rough, cauliflower-like $CeO_2$–$ZrO_2$ composites only using convenient and cheap precursors in the hydrothermal system without any surfactant or template. A series of experimental conditions, including time and temperature of hydrothermal reaction, calcination temperature and the concentration of precursors were investigated. Apparent morphological variations were observed by adjusting the time hydrothermal reaction. As the mineralizer, urea played an important role in the formation and morphology evolution of the $CeO_2$–$ZrO_2$ composites nanostructures. Based on the data of XRD, XPS and BET, and according to the images of SEM and TEM and other analysis, the mechanism was proposed to account for the structural dynamics and morphological evolutions going through the nucleation, Ostwald ripening and Kirkendall effect. We also found the $Ce_{0.9}Zr_{0.1}O_2$–GO hybrids have rather better adsorption for RhB than the sample without GO and the sample $CeO_2$, which may provide a good strategy for rapid control of pollutants. The results of this paper would provide an economical and stable route for synthesis of nanosized $CeO_2$–$ZrO_2$ composites and related materials and the detailed mechanism to narrate the morphology evolutions might serve as a new strategy for the controlled synthesis of functional nanocomposites in the future.

## References

1 G. Jacobs, L. Williams, U. Graham, D. Sparks and B. H. Davis, *J. Phys. Chem. B*, 2003, **107**, 10398.
2 F. Goubin, X. Rocquefelte, M.-H. Whangbo, Y. Montardi, R. Brec and S. Jobic, *Chem. Mater.*, 2004, **16**, 662.
3 A. Varez, E. Garcia-Gonzalez and J. Sanz, *J. Mater. Chem.*, 2006, **16**, 4249.
4 A. M. Efstathiou and S. Y. Christou, Catalytic Science Series vol. 12, in *Catalysis by Ceria and Related Materials*, ed. A. Trovarelli and P. Fornasiero, Imperial College Press, 2nd edn, 2013, vol. 3, ch. 3 – Investigation of the Oxygen Storage and Release Kinetics of Model and Commercial Three-Way Catalytic Materials by Transient Techniques, p. 139.
5 M. Adamowska, S. Muller, P. Da Costa, A. Krzton and P. Burg, *Appl. Catal., B*, 2007, **74**, 278.
6 K. B. Zhou, X. Wang, X. M. Sun, Q. Peng and Y. D. Li, *J. Catal.*, 2005, **229**, 206.
7 M. Daturi, E. Finocchio, C. Binet, J. C. Lavalley, F. Fally and V. Perrichon, *J. Phys. Chem. B*, 1999, **103**, 4884.
8 M. Daturi, N. Bion, J. Saussey, J.-C. Lavalley, C. Hedouin, T. Seguelong and G. Blan-chard, *Phys. Chem. Chem. Phys.*, 2001, **3**, 252.
9 R. Zhang, W. Y. Teoh, R. Amal, B. Chen and S. Kaliaguine, *J. Catal.*, 2010, **272**, 210.
10 M. Daturi, E. Finocchio, C. Binet, J.-C. Lavalley, F. Fally, V. Perrichon, H. Vidal, N. Hickey and J. Kaspar, *J. Phys. Chem. B*, 2000, **104**, 9186.
11 Z. Wang, Z. Qu, X. Quan and H. Wang, *Appl. Catal., A*, 2012, **411–412**, 131.
12 H. Vidal, J. Kašpar, M. Pijolat, G. Colonb, S. Bernal, A. Cordón, V. Perrichon and F. Fally, *Appl. Catal., B*, 2000, **27**, 49.
13 I. Atribak, N. Guillén-Hurtado, A. Bueno-López and A. García-García, *Appl. Surf. Sci.*, 2010, **256**, 7706.
14 B. M. Reddy, P. Lakshmanan, A. Khan, C. L. Cartes, T. C. Rojas and A. Fernandez, *J. Phys. Chem. B*, 2005, **109**, 1781.
15 H. R. Radfarnia and M. C. Iliuta, *Ind. Eng. Chem. Res.*, 2012, **51**, 10390.
16 S. Stankovich, *et al.*, *Nature*, 2006, **442**, 282.
17 S. R. Kim, M. K. Parvez and M. Chhowalla, *Chem. Phys. Lett.*, 2009, **483**, 124.
18 H. Zhang, X. J. Lv, Y. M. Li, Y. Wang and J. H. Li, *ACS Nano*, 2010, **4**, 380.

19 H. X. Mai, L. D. Sun, Y. W. Zhang, R. Si, W. Feng, H. P. Zhang, H. C. Liu and C. H. Yan, *J. Phys. Chem. B*, 2005, **109**, 24380.

20 G. Shen, Q. Wang, Z. Wang and Y. F. Chen, *Mater. Lett.*, 2011, **65**, 1211.

21 Q. Wang, C. H. Li, M. Guo, C. W. Hu and Y. C. Xie, *J. Mater. Chem. A*, 2014, **2**, 1346.

22 A. Vantomme, Z. Y. Yuan, G. H. Du and B. L. Su, *Langmuir*, 2005, **21**, 1132.

23 L. Yan, X. R. Xing, R. B. Yu, J. X. Deng, J. Chen and G. R. Liu, *Phys. B*, 2007, **390**, 59.

24 J. F. Li, G. Z. Lu, H. F. Li, Y. Q. Wang, Y. Guo and Y. L. Guo, *J. Colloid Interface Sci.*, 2011, **360**, 93.

25 L. R. Li and W. Z. Wang, *Solid State Commun.*, 2003, **127**, 639.

26 J. H. Liang, Z. X. Deng, X. Jiang, F. L. Li and Y. D. Li, *Inorg. Chem.*, 2002, **41**, 14.

27 H. R. Radfarnia and M. C. Iliuta, *Ind. Eng. Chem. Res.*, 2012, **51**, 10390.

28 M. Alifanti, B. Baps, N. Blangenois, J. Naud, P. Grange and B. Delmon, *Chem. Mater.*, 2003, **15**, 395.

29 E. Moretti, M. Lenarda, P. Riello, L. Storaro, A. Talon, R. Frattini, A. R. Carmona, A. Jiménez-López and E. Rodríguez-Castellón, *Appl. Catal., B*, 2013, **129**, 556.

30 Q. Yuan, Q. Liu, W. G. Song, W. Feng, W. L. Pu, L. D. Sun, Y. W. Zhang and C. H. Yan, *J. Am. Chem. Soc.*, 2007, **129**, 6698.

31 S. W. Yang and L. Gao, *J. Am. Chem. Soc.*, 2006, **128**, 9330.

32 S. Carrettin, P. Concepción, A. Corma, J. M. López Nieto and V. F. Puntes, *Angew. Chem., Int. Ed.*, 2004, **43**, 2538.

33 R. Si, Y. W. Zhang, S. J. Li, B. X. Lin and C. H. Yan, *J. Phys. Chem. B*, 2004, **108**, 12481.

34 B. Azambre, I. Atribak, A. Bueno-López and A. García-García, *J. Phys. Chem. C*, 2010, **114**, 13300.

35 Z. K. Zhao, X. L. Lin, R. H. Jin and Y. T. Dai, *Catal. Commun.*, 2011, **12**, 1448.

36 Z. K. Zhao, X. L. Lin, R. H. Jin and Y. T. Dai, *Catal. Sci. Technol.*, 2012, **2**, 554.

37 B. M. Reddy, P. Bharali, P. Saikia, G. Thrimurthulu, Y. Yamada and T. Kobayashi, *Ind. Eng. Chem. Res.*, 2009, **48**, 453.

38 L. J. Liu, Z. J. Yao, B. Liu and L. Dong, *J. Catal.*, 2010, **275**, 45.

39 S. Pengpanich, V. Meeyoo, T. Rirksomboon and K. Bunyakiat, *Appl. Catal., A*, 2002, **234**, 221.

40 S. M. Liu, L. M. Gan, L. H. Liu, W. D. Zhang and H. C. Zeng, *Chem. Mater.*, 2002, **14**, 2427.

41 C. J. Jia and L. D. Sun, *Angew. Chem., Int. Ed.*, 2005, **44**, 4328.

42 Y. Xiong, Y. Xie, J. Yang, R. Zhang, C. Wu and G. J. Du, *J. Mater. Chem.*, 2002, **12**, 3712.

43 J. Zhan, Y. Bando, J. Hu and D. Golberg, *Inorg. Chem.*, 2004, **43**, 2462.

44 M. Hirano and M. Inagaki, *J. Mater. Chem.*, 2000, **10**, 473.

45 H. G. Yang and H. C. Zeng, *J. Phys. Chem. B*, 2004, **108**, 3492.

46 Y. Chang, J. J. Teo and H. C. Zeng, *Langmuir*, 2005, **21**, 1074.

47 K. Huang, M. Lei, Y. J. Wang, C. Liang, C. X. Ye, X. S. Zhao, Y. F. Li, R. Zhang, D. Y. Fan and Y. G. Wang, *Powder Diffr.*, 2014, **29**, 8.

48 R. C. R. Neto and M. Schmal, *Appl. Catal., A*, 2013, **450**, 131.

# One Step Hydrothermal Synthesis of CeO$_2$-ZrO$_2$ Nanocomposites and Investigation of the Morphological Evolution

Xiaohui Zhang [a,b], Qiang Wang [a,b,*], Jing Zhang [a,b], Jigang Wang [a,b], Ming Guo [a,e], Shaowei Chen [c,*], Chunhong Li [d], Changwen Hu [e] and Youchang Xie [f]
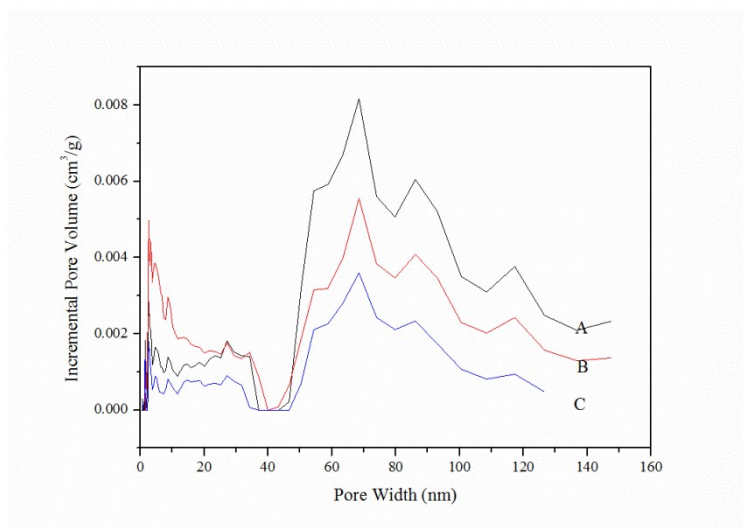
## Supporting information



Fig. S1 The pore size distribution: Ce$_{0.9}$Zr$_{0.1}$O$_2$ hydrothermal treated at 373K for A: 10 h, B: 24 h , C: 48 h then calcined at 673K.
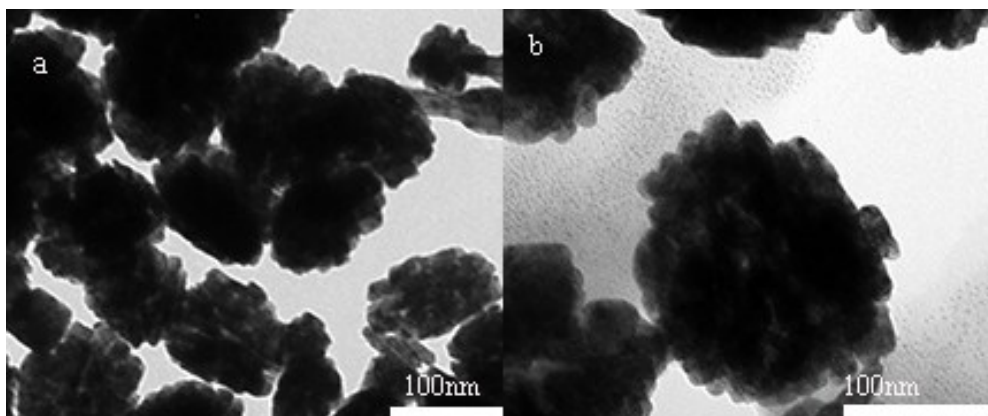


Fig. S2 CeO$_2$ hydrothermal treated at 373K for 48 h then calcined at 673K.
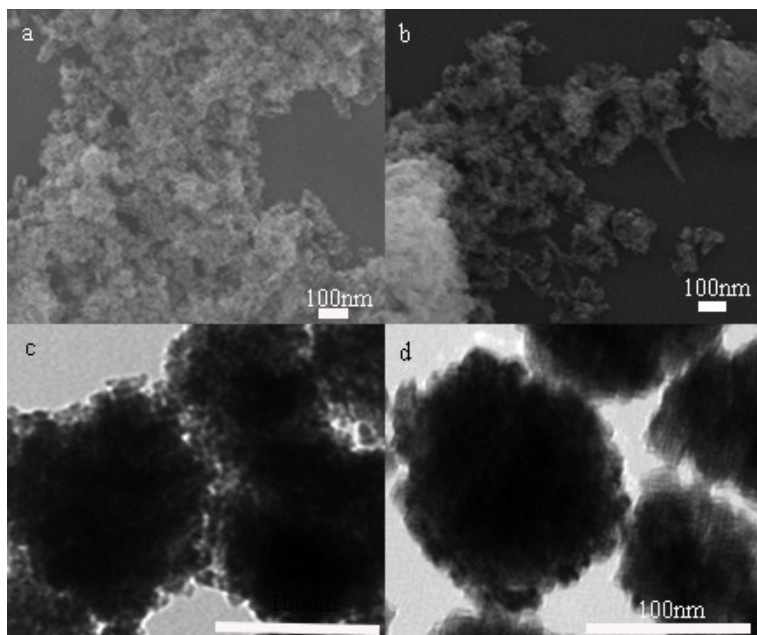
Fig. S3 The molar ratio of urea to precursor was 30:1 after hydrothermal treated at
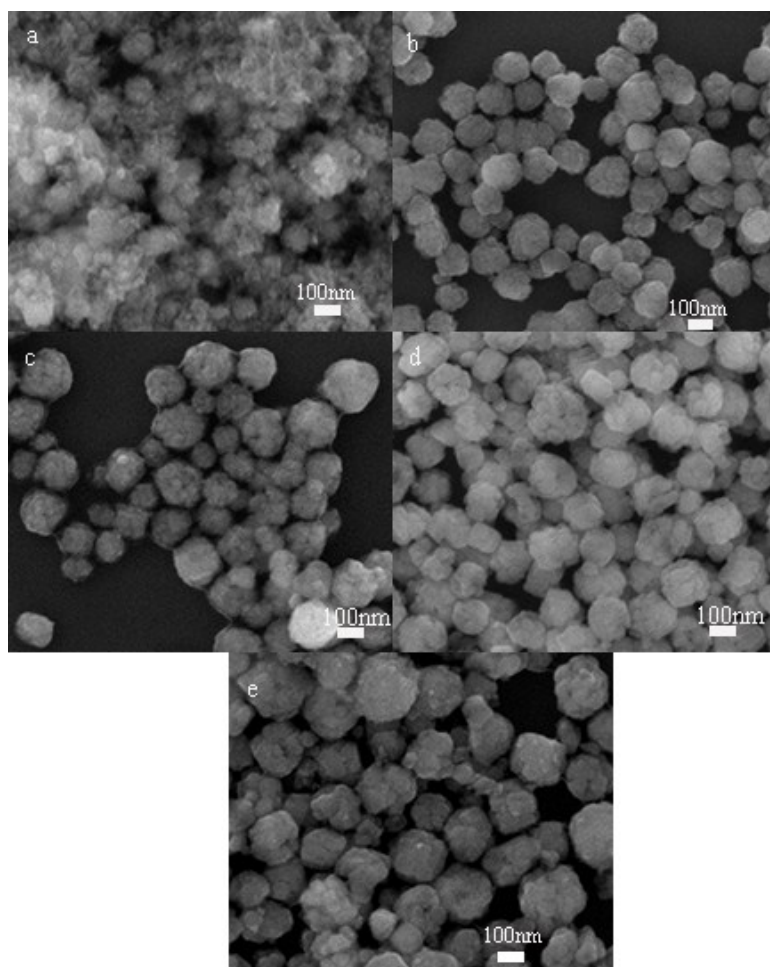
373K for (a) 4 h, (b)8 h, (c)10 h, (d) 15 h.

Fig. S4 The molar ratio of urea to precursor was 40:1 and hydrothermal treated at (a) 393K, (b) 413K, (c) 433K, (d) 453K, (e) 473K for 4 h.
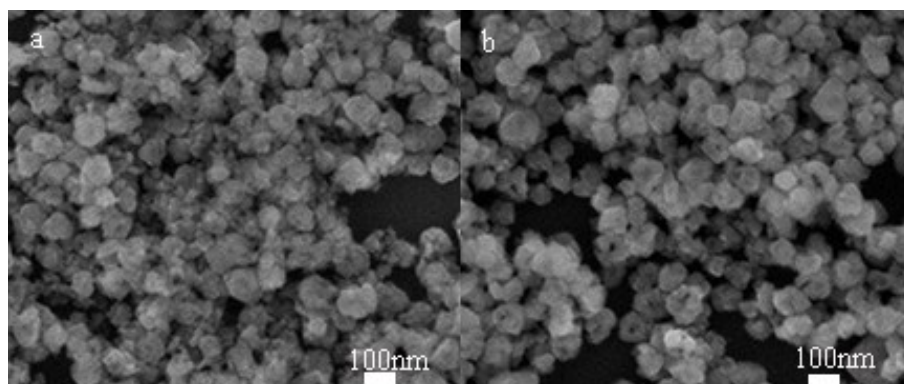


Fig. S5 SEM images of $Ce_{0.9}Zr_{0.1}O_2$ calcined at 1173K with the molar ratio of urea to precursor was 40:1 and hydrothermal treated for (a) 10 h, (b) 48 h.



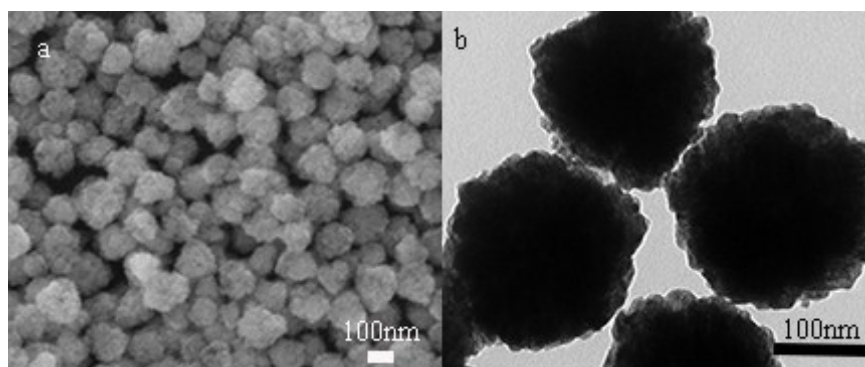Fig. S6 (a) SEM images of $Ce_{0.75}Zr_{0.25}O_2$ synthesized at 373K of 48h and calcined at 773K; (b) TEM images of $Ce_{0.75}Zr_{0.25}O_2$ synthesized at 373K, 48 h and calcined at 773K.

Briefly, 0.2 g of $CeO_2$ and $Ce_{0.9}Zr_{0.1}O_2$ were first added into the calculated amount of GO ( 8wt%) solution followed by ultrasonic dispersion for 30 min and vigorous stirring for another 2 h to disperse $CeO_2$ and $Ce_{0.9}Zr_{0.1}O_2$ sufficiently. Then, the mixing solution was transferred into a 100 ml Teflon-sealed autoclave at 423K for 5 h and cooled down to room temperature naturally. The resulting hybrids were recovered by centrifugation, washed with water and alcohol several times, and fully dried in air

at 333K.